Geomagnetism, Aeronomy and Space Weather:

A Journey from the Earth's Core to the Sun

Contents

Illustrations

Tables

Contributors

1
Chapter 1

This is for chapter 1

2

Chapter 2

This is for chapter 2

3
Chapter 3

This is for chapter 3

4
Chapter 4

This is for chapter 4

5
Chapter 5

This is for chapter 5

6

Chapter 6

This is for chapter 6

7
Chapter 7

This is for chapter 7

8
Chapter 8

This is for chapter 8

9
Chapter 9

This is for chapter 9

10
Chapter 10

This is for chapter 10

11
Chapter 11

This is for chapter 11

12
Chapter 12

This is for chapter 12

13
Chapter 13

This is for chapter 13

14
Chapter 14

This is for chapter 14

15
Chapter 15

This is for chapter 15

16

Chapter 16

This is for chapter 16

17
Chapter 17

This is for chapter 17

18
Chapter 18

This is for chapter 18

19

Long and short term geomagnetic prediction

Prediction of geomagnetic variability depends on the accuracy of geomagnetic field modeling, dynamical modeling of source regions that contribute to geomagnetic signals, and advanced assimilation algorithms that combine effectively the results of geomagnetic field and dynamic models to make accurate estimates of the dynamic states of the sources and, therefore, accurate forecast of geomagnetic variations. In this chapter we provide an overview of recent research efforts in these three research areas, focusing primarily on geomagnetic variations from the dynamic outer core and from solar and lunar tidal effects, but also including a review of relevant research results and developments. Prediction of weak but periodic tidal phenomena, and of strong but chaotic secular variation (SV) showcases two very important new developments which will lead to new opportunities in geomagnetic research and application.

19.1 Introduction

Geomagnetic data measured on the Earth's surface and in the low Earth orbits (LEO) show contributions from various sources within the Earth system and of external origins. Several examples can be found in other chapters of this book. These contributions depend on chemical and dynamical properties of the source regions. Therefore, observed geomagnetic variations provide important information for understanding the Earth system, and thus a means to monitor magnetically changes of the Earth system in space and in time.

Generally speaking, prediction and forecast of geomagnetic variations from a particular source region, e.g. the Earth's outer core, requires assimilation of observations into relevant dynamical models. Thus it in-

volves parallel efforts in dynamical models of the source region, geomagnetic field models to extract contributions of the source region from surface observations, and efficient assimilation algorithms (in both information acquisition and computational need). But they also complement each other: for example, results from the field models are used to constrain the dynamical models so that they can make better estimation of the "true" state (more accurately, the partial truth specified by the observations); and the improved dynamical models can be also used to assist the field models for more accurate source separations. This very simple description of geomagnetic prediction should therefore be fully explored for future geomagnetic research and application.

In this chapter, we focus on prediction of geomagnetic variation from two very different systems: geomagnetic secular variation (SV) from the convective outer core, and magnetic anomalies from tidal effects. They represent two extreme cases of geomagnetic variability: the former is dominantly strong (over 95% of energy) in the geomagnetic measurements, but is chaotic (and difficult to predict) in nature; while the latter is extremely weak but highly regular (thus predictable) in its temporal variation patterns. In particular, prediction of SV from the core, and of geomagnetic fluctuations from ocean tidal flow are new developments in geomagnetic studies and applications, and therefore deserve special attentions of IAGA community.

Observed SV plays a crucial role in understanding the core dynamics: small changes observable at the surface are the manifestation of variations in the outer core dynamic state, such as the fluid velocity field (e.g. Kuang and Tangborn, 2015). Therefore, its complex spatial/temporal variation patterns are not predictable over extended periods of time (e.g. Kuang et al, 2009; Hulot et al, 2010). By relative contrast, geomagnetic fluctuations due to tidal phenomena are approximately 10^{-5} order in magnitude of that of the core field. They are very predictable since they are generated at phase-locked astronomical periods. However, it is expected or observed that solar heating effects (also included as "tidal" geomagnetic variations) are much less stationarity. Their contrasting variation patters require very different approaches in analyzing and interpreting the observed signals.

Prediction of SV could greatly help our understandings of fundamental dynamical properties for interpretation of the SV observable at the surface, the geodynamo and the dynamic state in the outer core, and the properties of in the deep interior. The principle of geodynamo is very simple: the core field is generated and maintained by the outer core

fluid motion, most likely the convection driven by gravitational energy released from secular cooling and differentiation of the Earth over geological time scales. But the dynamic details are still very unresolved. Numerical geodynamo simulation can provide a partial depiction of the core dynamics (Christensen et al, 2010), but is hampered by lack of resolution (due to limited computing resource) to reach Earth-like parameter regimes. On the other hand, geomagnetic observations provide direct evidences of complex spatial and temporal variation of the intrinsic field. But the observational evidence is also partial, limited by short measurement records and long distances to the outer core (the source region of SV). As suggested by recent research results (Aubert and Fournier, 2011; Aubert, 2014; Kuang and Tangborn, 2015), geomagnetic data assimilation can integrate partial information from both studies to obtain better estimates of the core state, and thus improving our understandings of the core dynamics and its implications for interactions and responses between the outer core and other components of the Earth.

Predictability of global geomagnetic signals due to ocean tides is supported by the agreement shown in independent descriptions derived from theoretical forward models and field models of observations (Tyler et al, 2003; Sabaka et al, 2015, 2016). These studies have recently opened an opportunity for using the tidal magnetic signals to probe ocean electrical conductivity, variability in ocean tidal processes, and mantle conductivity (Schnepf et al, 2015; Grayver et al, 2016, 2017; Tyler et al, 2017).

This chapter is organized as follows: an overview of geomagnetic field modeling is given in the next section, followed by sections discussing the tidal magnetic signals, geodynamo and geomagnetic data assimilation using an ensemble Kalman filter, SV prediction on decadal and longer time scales, and finally a concluding discussion.

19.2 Source separation in geomagnetic field modeling

This chapter concerns the forecasting of long and short time-scale geomagnetic fields. Provided with initial conditions, the partial differential equations (PDEs) and boundary conditions (BCs) governing a particular constituent of the geomagnetic field would produce a time series of magnetic fields that would likely diverge from what could be or is observed. This is due to several reasons including the inadequacy of the PDEs and BCs to properly describe reality, and the sensitivity of these

to initial conditions. If realistic forecasting is to be achieved, then the PDEs and BCs must interact with actual observations, which is the basis of data assimilation described in Section 19.4. However, near the Earth one finds a rich variation of current systems and any measurement of the magnetic field will be composed of a superposition of these sources. It should be clear that if one is interested in predicting the Earth's core field, then any geomagnetic data assimilation system (GDAS) should be presented with measurements of the core field, not, for example, with a measurement of the nightside ionospheric induced field. It is crucial then that some type of source separation mechanism be developed before any meaningful forecasting can take place.

This section will present a particular philosophy and methodology of field modeling that provides separation of field sources in an optimal way. The general classification of these models is of the "inverse" variety, which is to say that the geophysical parameters of a numerical model are inferred from measurements of the magnetic field. Furthermore, these models are mostly "empirical" in that they describe the variations and patterns of the observed magnetic field with generic mathematical functions while abiding by some physical restrictions. This is in contrast to the usual "forward" models, which are composed of the PDEs and BCs alluded to above and run in free form given some initial conditions, independent of measurements. The fusing of inverse and forward models provides the basis for GDAS.

There are two concepts of field modeling that should be understood: correlation and bias. The first occurs when the mathematical functions corresponding to each parameter or coefficient can describe some portion of the measurements or data space that other functions do. If the part of the data space described by the function, or its span, can also be described by a combination of the spans of all other functions, then the model is ill-posed and does not possess a unique solution. If the other extreme occurs where no other function can describe any part of the data space described by any other function, then the functions are orthogonal over the data space with a zero correlation and each parameter may be estimated independently. Usually there is a non-empty intersection between each pair of spans, but there is also part of each span that is unique, thus rendering a unique solution. This non-empty intersection of spans leads to correlation between the associated parameters. Bias, on the other hand, is a discrepancy between the estimated and true values of a parameter that cannot be eliminated by resampling and averaging over the data space and is usually due to errors of omission or commission.

A successful estimation approach will attempt to mitigate bias while taking correlation into account.

Two major methodologies have emerged in dealing with correlation in geomagnetic field modeling. For discussion purposes, consider the following simple linear model consisting of two sets of parameter vectors, $\mathbf{x}$ and $\mathbf{y}$, associated with basis functions that comprise the columns of matrices $\mathbf{A}$ and $\mathbf{B}$, respectively, describing the data vector of measurements $\mathbf{d}$ in the presence of a vector of additive error $\boldsymbol{\nu}$ whose mean is zero and covariance is the identity matrix, such that

$$\mathbf{d} = \mathbf{A}\mathbf{x} + \mathbf{B}\mathbf{y} + \boldsymbol{\nu}. \tag{19.1}$$

The first method, "sequential estimation", attempts to estimate the parameters in an arbitrary order, say $\mathbf{x}$ followed by $\mathbf{y}$, where $\mathbf{x}$ is estimated directly from $\mathbf{d}$ followed by $\mathbf{y}$ estimated from the residuals $\mathbf{d}-\mathbf{A}\tilde{\mathbf{x}}$, where the tilde indicates the estimate of $\mathbf{x}$. It can be shown that if the cycle is repeated with subsequent $\mathbf{x}$ being estimated from the latest residuals $\mathbf{d} - \mathbf{B}\tilde{\mathbf{y}}$ and $\mathbf{y}$ estimated from the latest residuals $\mathbf{d} - \mathbf{A}\tilde{\mathbf{x}}$, then this constitutes a dual-block Gauss-Seidel method that converges as long as the entire system is non-singular. However, there are pitfalls with this method in that 1) in practice, only a single iteration is often performed, 2) convergence can be very slow, and 3) the method can mask co-linearities between basis functions that lie in separate blocks.

The second method is "co-estimation" which attempts to estimate all parameters in a single inversion. This method can be understood by considering a data space D and the spans of the columns of matrices $\mathbf{A}$ and $\mathbf{B}$ within this space. The regions of intersection between the spans of $\mathbf{A}$ and $\mathbf{B}$, denoted "$A \cap B$", represent areas of dispute where both sets can describe the data and thus lead to non-uniqueness. In co-estimation, these regions are eliminated from consideration and the $\mathbf{x}$ and $\mathbf{y}$ parameters are rather determined from the unique regions of "$A \setminus B$" and "$B \setminus A$", respectively.

The error between a true model state $\mathbf{x}$ and its estimate $\tilde{\mathbf{x}}$ as measured by the mean-squared error (MSE) may be decomposed into two terms, as shown in the following equation, one involving bias $\mathbf{b}$ and the other involving variance $\mathbf{C}$

$$\begin{aligned} MSE\left(\tilde{\mathbf{x}}\right) &= E\left[\left(\tilde{\mathbf{x}} - \mathbf{x}\right)^{\mathrm{T}}\left(\tilde{\mathbf{x}} - \mathbf{x}\right)\right], \\ &= \mathbf{b}^{\mathrm{T}}\mathbf{b} + Tr\left[\mathbf{C}\right], \end{aligned} \tag{19.2}$$

where $E\left[\cdot\right]$ is the expectation operator, $Tr\left[\cdot\right]$ is the trace operator,

$\mathbf{b} = \mathbf{x} - \bar{\mathbf{x}}$, and $\bar{\mathbf{x}}$ and $\mathbf{C}$ are the expected value and covariance of $\tilde{\mathbf{x}}$, respectively. These two terms represent orthogonal contributions over the space of all estimates. In the case of least-squares estimation, the bias term is *assumed* zero and thus the model error is often reported only as the variance term. However, when modeling real magnetic fields this is surely never the case and in fact the bias term may actually dominate.

As with correlation, basically two approaches are used to minimize the effects of bias. The first is data selection in which subsets are chosen that do not contain an undesirable field constituent. For example, external fields exhibit a range of intensities and their presence can be detrimental to the resolution of fields from the core and lithosphere (see Finlay et al, 2017; Olsen and Stolle, 2017). Therefore, most models will use data from so-called "quiet times" when external fields are relatively weak. In another example, since the primary ionospheric field is mostly absent during the night sector, most models interested in the core and lithosphere will choose data during this time. However, because of the complexities of the magnetic environment, it is difficult to make data selections that eliminate all unwanted contaminates. For instance, when night sector data is chosen to filter out primary ionospheric signals, it turns out that the associated secondary or induced field is still present and this indeed biases estimates of the core field. This particular contaminate affects the odd, low-degree zonal terms of a spherical harmonic expansion of the core field.

The second approach entails co-estimating the biases, or nuisance parameters, along with the nominal parameters. The assumption is that there exists a subset of measurements whose signal-to-noise ratio is large enough to accurately resolve a particular subset of parameters. All other data subsets are not used to resolve these parameters. If this holds true, then a functional representation of the actual contaminate is not needed since only its projection onto the nominal basis functions comes into play leaving only nuisance versions of the nominal parameters of interest to be estimated. Using the example of night sector contamination by induced ionospheric fields, if day sector data is introduced, then a representation of this induced field may be estimated from the data. However, since the day sector data will be contaminated with respect to core and lithospheric fields, it is used to estimate nuisance versions of these. The result is that core and lithospheric field derived from night sector data are now not contaminated by ionospheric induction.

Some level of the co-estimation approach is followed by all modeling efforts, including the very successful POMME (Maus et al, 2006; Maus,

2017), GRIMM (Lesur et al, 2008, 2015a,b), and CHAOS (Olsen et al, 2014; Finlay et al, 2016) suites. However, the suite of "Comprehensive Models" (CMs) (Sabaka et al, 2002, 2004, 2015, 2016) in general attempt to co-estimate more sources. Aside from the usual core and lithospheric fields, these models have been able to simultaneously resolve the Solar Quiet (Sq) fields as well as the oceanic M_2 tidal field. As for biases, the CMs use limited data selection and employ the "Selective Infinite Variance Weighting" (SIVW) scheme of Sabaka and Olsen (2006) and Sabaka et al (2013), which essentially treat the biases in the manner described above. It is envisioned that an estimation scheme like that used in the CMs will be combined with geodynamo simulation algorithms as a front-end filter to provide a GDAS algorithm for improved long term geomagnetic forecasting.

19.3 Predictability of tidal phenomena in the geomagnetic record

When considering rapid temporal fluctuations around the slowly changing main field, one may anticipate high predictability resulting from phenomena driven by the Sun and Moon. The spin/orbits and gravitational potentials of the Earth, Moon, Sun, and even the radiation from the Sun, are all highly predictable. Modulations in the associated geomagnetic fluctuations may be expected then to primarily reflect temporal variations in the Earth's response to these "tidal" driving forces.

To describe the predictability of the tidal effects in the geomagnetic field, one can consider the long record of observations from the Honolulu (station HON) geomagnetic observatory. Specifically, the hourly-sampled records are differenced in time to produce the Eastward (E), Northward (N), and radial (R), vector-component time series.

In Figure 19.1 the power spectral density is shown (the spectrum is produced using the Welch averaging method on 24×1024-hour Hamming windowed segments). While one sees a red spectrum for periods longer than about a week, shorter-period power density increases and shows narrow spectral peaks. The larger of these peaks appear to be multiples of the Earth's rotation frequency with respect to the Sun, as well as frequencies derived from adding or subtracting pairs of such frequencies. This suggests that the variability may be predominantly due to solar radiation and gravity tidal forces under amplitude and phase modulation by the parameters involved in the Earth's response.

Empirical Orthogonal Functions (EOFs) compactly describe the variability in these time series in terms of statistical modes. The EOF analyses can be applied to the data matrix created as follows. Start by regarding $[E,\ N,\ R]$ as a 3-column matrix, each column representing a time series of hourly samples. It is then replaced with a 72-column matrix in which each row presents one day of data (the $1 \cdots 24$ hourly samples of the E, N, R, sequentially). In this case, the data matrix presents 72 time series of daily samples. While simply averaging this data matrix along the columns would give a 1×72 row vector describing the time-averaged behavior of E, N, R over the course of the solar day, such averaging could remove, or even cancel, components of regular signals with strong modulations due to seasons or other factors. The EOF analyses removes this limitation.

In the EOF analysis, the original 72 time series are linearly combined to produce 72 new time series. Each linear combination is referred to as an EOF mode, and the associated time series modulating the mode is referred to as the expansion coefficient series. The EOF modes and expansion coefficients are both orthogonal sets and have the useful property that the amount of total variance explained decreases monotonically from mode 1 to the higher modes. They are statistically most efficient at compactly describing the variance presented in the data matrix described above. The construction of the data matrix implicitly imposes a request for regular structures organized with respect to the solar day, as is the proximate goal.

In Figure 19.2 the results of the EOF analysis are shown. Remarkably, the first mode explains a fraction 0.48 of the variance and the second mode explains 0.14 such that more than half of the variance is captured in only two of the 72 EOF modes. Also important, there is a large drop and gradual decline in the variance explained by the higher modes, suggesting that other fluctuations in the data that are not particularly organized with respect to the solar day are simply being represented through this remaining part of the orthonormal expansion.

The EOF spectra, on its own, suggests much of the solar daily variability is captured in two modes. This is further supported by the EOFs shown in the upper right panels of Figure 19.2. The first two modes show well studied "solar-quiet" type curves with larger amplitudes during the local day time, and larger amplitudes in the horizontal components consistent with large-scale sheet currents overhead. The first two modes also appear in quadrature, suggesting one common process with phase migration.

The associated expansion coefficients (which modulate the EOF structures shown in the upper right panels) are also highly intuitive. Magnification shows a strong seasonal cycle in modes 1 and 2, which also appear in quadrature, suggesting again a common process with phase modulation. The low-pass curves show more clearly that there is also amplitude modulation with the solar cycle in modes 1 and 2. EOF mode 3 appears to also include influences due to the seasonal and solar cycles but the correspondence is less clear and other influences are also present.

While solar influences appear to dominate the spectral peaks, lunar periodicities are also clear on closer examination of the spectra. The M_2 semi-diurnal tide with a period of 12.42 hours is an example that can be seen to the left of the 1/2-day peak in Figure 19.1. Love and Rigler (2014) have conducted a careful and thorough spectral study of the HON time-differenced records using maximum-entropy and Lomb periodogram methods. They show and discuss solar, lunar, and lunisolar periodicities corresponding to astronomically established periods ranging from a couple hours to a couple decades. While both the Moon and the Sun are clearly involved in these tidal fluctuations in the magnetic field, from a single observatory it is not immediately clear if the tides involved are primarily in the ocean or upper atmosphere.

In the case of the M_2 constituent, comparison of observations with forward-modeled simulations have established that the magnetic field is primarily generated through motional induction by the ocean tidal flow. This can be seen in Figure 19.3 which shows the first frame of a movie (available at `https://neptune.gsfc.nasa.gov/gngphys/index.php?section=455`, and see Tyler et al (2003); Sabaka et al (2015, 2016) for further information). One may note that while the M_2 map derived from observations (middle panel) has spherical harmonic base functions that independently attempt to separate internal and external sources, both the ionospheric tides as well as the oceanic tides are below the satellite observatories, and the spatial coverage of land observatories is poor over the ocean regions. The simplest independent indication of the oceanic origin is in the correlation of amplitudes with ocean basins, and certainly the rough correspondence with the M_2 surface displacement is also indicative. The primary disagreement seen between the theoretical and observational M_2 fields is in the difference in spatial resolution. Whereas the theoretical simulations are conducted using the one sixth-degree lon./lat. resolution of the ocean tidal model data, the observations extend only to a much coarser resolution (up to the spherical-harmonic degree 18). With continued collection of satellite data, and improved

modeling, it is expected that the agreements between the models will either increase or reveal new physical effects.

Because only the gravitational (and not radiational) tidal forces by the Moon on the Earth are expected to be important, and because the gravitational tidal forces are known quite precisely, the lunar tidal forces can be regarded as highly predictable. Of course the tides that respond to these forces also depend on internal parameters and processes that may vary in time, with effects on the predictability of the response. On large scales, at least, the ocean fluid's tidal response can also be regarded as highly predictable (Egbert and Ray, 2017). Because the ocean electrical conductivity is also known from observations (Tyler et al, 2017), and is seen to have only very small temporal variations when considering offshore depth integrals, it is expected that ocean tidal magnetic fields may have a similarly high degree of predictability. In this case, the forward simulations such as shown in the middle panel of Figure 19.3 may be expected to reliably predict the tidal magnetic fields, including the high-spatial variations not yet confirmed by lower-resolution observational results such as shown in the bottom panel.

The magnetic fields motionally generated by lunar tidal forces on the ocean may present the most predictable, large-scale, naturally-occurring geomagnetic fluctuations. In this case, it is potentially an important source for sounding and/or monitoring the electrical conductivity of the oceans as well as the upper mantle. But the variability or even the stationarity of the ocean tidal magnetic fields has not yet been adequately examined, despite many observations demonstrating appreciable fluctuations in at least the tides of coastal observatories. In fact, the small observed variations in the M_2 surface height amplitude at coastal observatories, notably Honolulu (Colosi and Munk, 2006), have been closely studied as they may indicate changes in ocean parameters, processes, and stratification. Tyler (2013) presented a corresponding description of the history of M_2 variations seen in the magnetic observations at HON and showed that the fractional amplitude of the variability in the magnetic field is much higher than that seen in the sea surface displacement. This must be further studied to determine the stability of the tidal magnetic fields used as a sounding source.

19.4 Mathematics of geomagnetic data assimilation

Currently, there are many geodynamo models based on different physics and numerical schemes (Christensen et al, 2001; Jones et al, 2011; Matsui et al, 2016), and many different data assimilation algorithms (see, Kalnay 2017) . The mathematical description in this section is based on the formulations used in our geomagnetic data assimilation system (Jiang and Kuang, 2008; Kuang et al, 2008; Sun and Kuang, 2015). But they can be easily adapted to other geodynamo models. Note that all variables, unless otherwise specified, are non-dimensional in the rest of this chapter.

In our geodynamo model, the Earth's fluid outer core is approximated as a Boussinesq, electrically conducting fluid shell between the inner core boundary (ICB) with the mean radius r_{icb}, and the core-mantle boundary (CMB) with the mean radius r_{cmb}. The core state is described by the velocity field $\mathbf{v}$, the magnetic field $\mathbf{B}$ and the relative density anomaly $\delta\rho$. Since $\mathbf{v}$ and $\mathbf{B}$ are solenoidal, they can each be described by the two independent scalar fields, e.g.

$$\mathbf{B} = \mathbf{B}_T + \mathbf{B}_P \equiv \nabla \times (T_b \hat{\mathbf{r}}) + \nabla \times \nabla \times (P_b \hat{\mathbf{r}}) \tag{19.3}$$

where T_b and P_b are called the toroidal and poloidal scalars, respectively. These five scalar fields are approximated by spherical harmonic expansions, with the spectral coefficients defined on discrete radial grid points, e.g.

$$\begin{bmatrix} T_b \\ P_b \end{bmatrix} = \sum_{0 \le m \le l}^{L} \begin{bmatrix} j_l^m(r_i) \\ b_l^m(r_i) \end{bmatrix} Y_l^m(\theta, \phi) + C.C., \tag{19.4}$$

where Y_l^m are the spherical harmonic functions of degree l and order m, r_i are the radial grids, and $C.C.$ are the complex conjugate parts. The core state can be symbolically defined by a state vector $\mathbf{x}_d$ and is governed by the following initial-value problem

$$\begin{aligned} &\frac{\partial \mathbf{x}_D}{\partial t} = \mathbf{M}(\mathbf{x}_D, \Lambda), \\ &\mathbf{x}_D(t_0) = \mathbf{x}_d^0. \end{aligned} \tag{19.5}$$

where Λ denotes the dynamo parameters arising from model scaling rules and describing the outer core properties, such as the small magnetic Rossby number R_o (for the fluid inertia) and the small Ekman number E (for the viscous effect). For the details of (19.5) and the dynamo parameters, we refer the reader to (Kuang and Bloxham, 1999; Kuang and Chao, 2003, e.g.).

In geomagnetic data assimilation, the model output $\mathbf{x}_D$ is called the

forecast (and denoted by $\mathbf{x}^f$ in the rest of the section). In sequential data assimilation, the forecast $\mathbf{x}^f$ is modified at the time t_a when observations $\mathbf{y}$ are made:

$$\mathbf{x}^a = \mathbf{x}^f + \mathbf{K} \cdot \left(\mathbf{y} - \mathbf{H} \cdot \mathbf{x}^f \right), \tag{19.6}$$

where $\mathbf{K}$ is called the gain matrix, and $\mathbf{H}$ is the observation operator which projects the model space to the observation space (the two are in general different). The modified state $\mathbf{x}^a$, called the analysis, is then used as the initial state for making the forecast at $t > t_a$ via (19.5). The gain matrix $\mathbf{K}$ is chosen to minimize the (weighted) differences between $\mathbf{x}^a$ and $\mathbf{x}^f$, and between $\mathbf{x}^a$ and $\mathbf{y}$, and is of the form

$$\mathbf{K} = \mathbf{P}^f \mathbf{H}^T \left(\mathbf{H} \mathbf{P}^f \mathbf{H}^T + \mathbf{R} \right)^{-1}, \tag{19.7}$$

where $\mathbf{P}^f$ and $\mathbf{R}$ are the error covariances of the forecasts and of the observations, respectively. In the ensemble Kalman filter (EnKF) approach (e.g. Kalnay, 2011), $\mathbf{P}^f$ is determined with an ensemble $\left\{ \mathbf{x}_i^f | i \leq N \right\}$ of forecasts:

$$\mathbf{P}^f = \left\langle \left(\mathbf{x}^f - \overline{\mathbf{x}}^f \right) \left(\mathbf{x}^f - \overline{\mathbf{x}}^f \right)^T \right\rangle, \qquad \overline{\mathbf{x}}^f = \frac{1}{N} \sum_{i=1}^{N} \mathbf{x}_i^f, \tag{19.8}$$

where $\langle \cdot \rangle$ implies the ensemble average. Through repeated processes, it is expected to pull the geodynamo model (19.5) closer to the truth, i.e. to reduce the difference between the forecast $\mathbf{x}^f$ and the true core state $\mathbf{x}^t$ (not really known) in time.

Often approximations are made to $\mathbf{P}^f$ to reduce computational cost or to deal with unknown state properties, e.g. modeled (or parameterized) $\mathbf{P}^f$ in the optimal interpolation (OI) approach (e.g. Kalnay, 2011). Both approaches are used in our geomagnetic data assimilation system (e.g. Kuang et al, 2008; Sun and Kuang, 2015; Tangborn and Kuang, 2015).

In geodynamo simulation, the truncations are typically of order 10^6 (or 5×10^6 parameters to define the core state). But surface geomagnetic measurements can obtain the poloidal coefficients b_l^m up to the degree $L_{obs} \leq 13$ (e.g. Langel, 1987), or slightly better $L_{obs} \leq 20$ for SV (e.g. Langel, 1987; Finlay et al, 2016), mainly due to the spatial attenuation between the CMB and the surface, and due to the contamination of the crustal field, leading to approximately an order 10^5 differences between the coefficients from the dynamo models and from the observations. Therefore, the observation operator $\mathbf{H}$ is very simple and very sparse. If

denoting by H_{ij} the elements of $\mathbf{H}$, then,

$$H_{ij} = \delta_{ip}\delta_{jq}, \tag{19.9}$$

where the index pairs (p, q) are defined by $\{b_l^m(r_d)|0 \leq m \leq l \leq 20\}$.

19.5 Geomagnetic SV prediction

19.5.1 An overview

There are has been a long history of SV prediction in geomagnetic research and application. Perhaps the best examples are the 5-year predictive models included in the International Geomagnetic Reference Field (IGRF). These models are defined by the SV Gauss coefficients that are time-invariant in the forecast period. Prior to IGRF−11, they were produced via some optimal mathematical extrapolation of the Gauss coefficients obtained from prior geomagnetic measurements (e.g. Maus et al, 2005). Starting from IGRF−11, the predictive models also include contributions from two new approaches: the forecast based on the core flow inverted from geomagnetic observations (Maus et al, 2008; Beggan and Whaler, 2009; Gillet et al, 2013, 2015; Whaler and Beggan, 2015; Barrois et al, 2017), and the forecast made by assimilation of past geomagnetic observations into geodynamo models (Kuang et al, 2010; Fournier et al, 2015).

In the former approach, the forecast is made based on the non-diffusive magnetic induction at the CMB, with the fluid velocity field also derived from the observed SV. Therefore this approach can be characterized as "data-driven" and "kinematic" (or partially dynamic) in nature. In the latter approach, core dynamics models are determined independently from any observations. These models and surface geomagnetic observations provide two independent estimates of the SV. And the assimilation algorithm employed in this approach works to optimally utilize the two independent assessments for making improved SV forecast. Therefore, the latter is called the geomagnetic data assimilation (GDAS), and is the focus of this section. Since the two approaches share many common methodologies and concerns, such as the stochastic EnKF analysis, the discussion in this section is also applicable to the first approach.

19.5.2 Decadal SV prediction

Initial work in GDAS began with observing system simulation experiments (OSSEs), in which synthetic observations are created by a model, and are assimilated into the same model with some parameter differences. The first two were performed with very similar one-dimensional MHD models that mimic the nonlinear geodynamo process (Sun et al, 2007; Fournier et al, 2007), with sparse observations taken from the full system. These two experiments, one based on an ensemble Kalman-filter algorithm (Sun et al, 2007) and the other on the variational approach (Fournier et al, 2007), demonstrated that assimilation of the sparsely distributed data can bring the forecasts closer to the true state of the system. They also highlighted the differences between sequential and variational data assimilation algorithms. The former has the advantage of relatively simple implementation, since they do not require the construction of a tangent linear model (TLM) or it's adjoint. The latter has the potential to improve estimates of earlier states of the core, when there were relatively sparse observations available for assimilation. Most of recent development work has involved sequential algorithms. But there has been recent progress in variational methods as well (Canet et al, 2009; Li et al, 2011, 2014).

Liu et al (2007) carried out OSSEs with two different fully nonlinear and three-dimensional geodynamo models separated by two different Rayleigh numbers. In their experiments, the synthetic data were generated at the CMB (i.e. the boundary) from one dynamo solution; while the other model was used for assimilation. Their results further confirmed that similar conclusions can be drawn for fully nonlinear geodynamo models. These experiments partially addressed a fundamental concern on whether geomagnetic observations, only available to a portion of the poloidal magnetic field at the CMB, could be used to improve model estimation (i.e. the full geodynamo solution) of the true core state which can then be used to make accurate geomagnetic forecasts.

Since then, numerous studies have furthered our knowledge of GDAS, and our capabilities to probe core dynamical processes and to make accurate SV forecasts. For example, Kuang et al (2009), Fournier et al (2010) and Hulot et al (2010) worked on understanding the geomagnetic forecast time limit. Aubert and Fournier (2011), Aubert (2014), Fournier et al (2011), Kuang and Tangborn (2015), and Tangborn and Kuang (2015) used GDAS to probe dynamical processes in deep outer core that are consistent with geomagnetic observations and to understand statisti-

cal properties of geodynamo solutions. In particular, Kuang et al (2010) and Fournier et al (2015) used GDAS to provide 5−year predictive geomagnetic candidate models for IGRF. More recently, efforts have been made on prediction of longer-term geomagnetic variability, including reversals (Morzfeld et al, 2017; Tangborn and Kuang, 2018). It should be pointed out, most of the GDAS systems currently in use are based on EnKF algorithms Fournier et al (2011) (see also Section 19.4 for the mathematical details). This approach retains covariances between different state variables, thus enabling corrections to unobserved variables.

Despite the progress made thus far, we are still facing many challenges in GDAS. One is the excessive computational expense arising from large ensemble sizes used in the EnKF, such as those computation with as many as 500 model simulations by Fournier et al (2013), which is prohibitive for experiments that might encompass thousands of years of Earth core dynamical processes. An alternative is to develop modeled covariances Tangborn and Kuang (2015) validated using observation minus forecast (O-F) statistics, though the changes to the unobserved are made indirectly through the model and therefore take longer. A compromise approach that could utilize the best of the two is perhaps a hybrid of the ensemble-generated and modeled covariances (Hammill and Snyder, 2000), which would allow a much smaller ensemble size while retaining the cross covariances. It should be also pointed out that approaches utilizing simplified core dynamics models (e.g. Jault, 2008; Canet et al, 2009) can also help bring down the computing expense. But, as discussed in the following, simplified models could potentially produce larger model biases.

Another critical issue is the sparsity of the geomagnetic data (see Section 19.4). This will remain for a very long time. Utilization of archeomagnetic and paleomagnetic data (e.g. Korte and Constable, 2011; Licht et al, 2013; Nilsson et al, 2014) will be discussed in the following subsection. Efforts should be also on assimilation of derived products from geomagnetic measurements, and non-geomagnetic data relevant to core dynamics. For example, observed SV could potentially increase the available data by an order of magnitude (Kuang and Tangborn, 2015), and length-of-day (LOD) and polar motion variation on decadal time scales that are from core-mantle angular momentum exchanges (Jault et al, 1988; Holme and Whaler, 2001; Gillet et al, 2010; Kuang et al, 2017) could provide additional constraints on the (unobserved) toroidal field $\mathbf{B}_T$ at the CMB. Utilization of these new data will bring complex and even nonlinear observation operator $\mathbf{H}$ to GDAS.

The EnKF algorithm depends on the error statistics of geomagnetic observations (e.g. geomagnetic field models), and of core dynamics (e.g. geodynamo models). Geodynamo model error statistics are approximated by the forecast covariance matrix $\mathbf{P}^f$ in (19.7) (Fournier et al, 2013, 2015; Sun and Kuang, 2015). Similar covariances are also provided in recent geomagnetic field models (e.g. Gillet et al, 2013; Licht et al, 2013; Nilsson et al, 2014). However, these are far from satisfactory because $\mathbf{P}^f$ could only provide knowledge of the distribution, but not the bias of the ensemble. Such biases can exist in both the field modeling (see Section 19.2) and in geodynamo models (Kuang et al, 2010), due to different physics and mathematics employed in the models. For example, geodynamo model biases are from different physics/hypotheses (e.g. boundary conditions discussed by Kuang and Bloxham (1997) and Sakuraba and Roberts (2009), different parameter regimes (e.g. Christensen et al, 2010; Aubert et al, 2017) which affect the scaling rules (e.g. Kuang et al, 2008; Aubert, 2014) used in GDAS. Comprehensive investigations may require large ensembles of the models with different physics and mathematics in different parameter domains.

Rescaling numerical dynamo models for GDAS will remain for many years since, due to computational constraint, the numerical parameters in dynamo simulation are several orders of magnitude away from those appropriate for the Earth's core. Mathematically, this implies that the scaled magnetic field $\mathbf{B}/\mathcal{B}$ will be used for assimilation. The scaling factor $\mathcal{B}$ can be obtained in different means. One approach, first adopted by Aubert (2014), is to define $\mathcal{B}$ with the asymptotic scaling rules derived from geodynamo solutions (Christensen et al, 2010). Kuang et al (2008) took a much simpler approach by making $\mathcal{B}$ the time-averaged magnitude of $\mathbf{B}$. This approach performs surprisingly well as it is not sensitive to model parameters (similar to the asymptotic scaling rules). To better explain this, consider the following quantity

$$\delta B \equiv \left(|\mathbf{B}| - \mathcal{B}\right)/\mathcal{B}, \tag{19.10}$$

where $|\mathbf{B}|$ is the *rms* magnetic field in the outer core (and $\mathcal{B}$ is therefore the time-average of $|\mathbf{B}|$). As shown in Table 19.1, the mean $\mathcal{B}$ varies strongly with the Rossby number R_o: it decreases by more than a factor of 4 from $R_o = 2.5 \times 10^{-6}$ to $R_o = 3.125 \times 10^{-7}$. However, the standard deviation $\sigma(\delta B)$ remains nearly unchanged in the all Rossby numbers. Similar properties are also found for the poloidal field $\mathbf{B}_P$ at the CMB (but with slightly smaller R_o).

But the time scalings are more complicated. From the power spectra

Table 19.1 *The mean $\mathcal{B}$ and the standard deviation $\sigma(\delta B)$ for different Rossby numbers R_o.*

R_o	2.5×10^{-5}	1.25×10^{-6}	6.25×10^{-7}	3.125×10^{-7}
$\mathcal{B}$	1.2356	0.4635	0.3225	0.2869
$\sigma(\delta B)$	0.0697	0.0877	0.0602	0.0767

of δB and of δB_P for the poloidal field at the CMB (in Figures 19.4), one can find that the power spectra for $R_o \geq 1.25 \times 10^{-6}$ (green and red curves) are significantly different from those for $R_o \leq 6.25 \times 10^{-7}$ (blue and black curves). In particular, the latter two are very similar, suggesting asymptotic convergences in the frequency domain in the poloidal field at the top of the $D''-$layer, bringing a hope to find a parameter-independent, dynamical consistent time scale for all dynamo solutions used in GDAS with $R_o \leq 6.25 \times 10^{-7}$. Similar properties are also shown in the total magnetic field anomaly δB of $\mathbf{B}$ in the outer core (but is not shown here). It should be pointed out that the frequency domain in 19.4 is controlled by the time steps and the output settings of our simulation. Further numerical analysis is needed to investigate variations with even higher frequencies. However, these figures are sufficient for our current discussion. We should point out also that similar analysis on time scales was done by others, e.g. Bouligand et al (2016) analyzed statistical properties of dynamo fields with different parameter values and compared to those from observations.

19.5.3 Millennial and longer SV prediction

Many of the important physical processes in the Earth's core take place on time scales of thousands of years or longer. This means that in order to capture core dynamics in any meaningful way in a geomagnetic data assimilation system, it is essential to assimilate data from epochs dating long before direct measurements of the geomagnetic field begain. An extreme example of this involves using a scaler stochastic model over millions of years that assimilates paleomagnetic data over this time frame. Morzfeld et al (2017) showed that this can lead to prediction of future dipole reversals as far as 4000 years in the future. But this type of model does not give any insight into the physical processes within the Earth's core that trigger the reversals. This requires a fully three-dimensional

geodynamo model, which is at present too computationally intensive to be feasible on these very long timescales. But intermediate assimilation experiments on the order of thousands of years are now possible, and recent work has been carried out on these. For example, Sanchez et al (2016) used a geodynamo model to produce a geomagnetic field model over an 800 year period with archeomagnetic data as observations in a data assimilation system. The resulting field model is constrained by the physics of the geodynamo model rather than the regularization and smoothing used in traditional field models.

Another approach is to assimilate traditional field model outputs into a geodynamo model over longer periods of time. For this we need to include the indirect paleo- and archeomagnetic measurements. These are made from lava flows and marine sediments, as well as fired clay bricks or other human artifacts, respectively (Donadini et al, 2009). This type of data contains one or more of magnetic inclination, declination and intensity values, and are relatively more frequent during the last 3000 years. All of these data sources are parametrized in terms of spherical harmonic expansions spatially, and B-splines temporally. Field models are generally divided by the type of data that they incorporate. The *CALS3k.4* model (Korte and Constable, 2011), which is based on both and paleo- and archeomagnetic data available for the last three thousand years, but is also constrained by *gufm1* (Jackson et al, 2000) for the last 400 years of the model.

The information available from this early era in the *CALS3k.4* model make it valuable for the study of longer time scales changes. The more direct measurements are incorporated into the *gufm1* model (1590 to 1990), which make use of the sailing ship compass records and magnetic observatory data starting in the mid 19th century until present. The CM4 model (Sabaka et al, 2004) (1960 to 2002) uses satellite measurements from a variety of missions, allowing it to include smaller spatial scale structures of the field. The accuracy of these models naturally improves during later times, which can be attributed to both a better spatial distribution and data precision, as well as the progress in separating the different sources that contribute to the observed field. Tangborn and Kuang (2018) have used data assimilation to connect these 3 field models via a geodynamo model. The purpose of this work was to show how data assimilation can be used to obtain independent estimates of errors in the *CALS3k.4* model from a long assimilation run that ends with the CM4 model in 1990.

It presented a series of nearly 2000 year geomagnetic data assimilation

experiments that use the *CALS3k.4* field model as observations from 10 CE to 1590 CE, followed by *gufm1* (1590-1950) and CM4 (1970-1990). In each epoch, the field models were assimilated into the geodynamo model every 20 years. The goal was to use the higher accuracy of *gufm1* and CM4 to gain additional insight (beyond the estimates provided with the field model) into the precision of *CALS3k.4*, particularly as the maximum degree L assimilated is varied. These independent estimates of the uncertainty in the field models used a simple relationship for the Gauss coefficients. The error standard deviation, $(\sigma^o)_l^m$, in each was modeled as being proportional to its magnitude, $(\sigma^o)_l^m = \alpha^o||b_l^m$, where α^o is the observation error coefficient up to $L =$. For higher degrees, larger errors were assigned that essentially removed the observations from the assimilation. Smaller errors are assigned after 1590 when sailing ship data become available, along with observatory data in the 19^{th} century, and satellite data after 1960.

Tangborn and Kuang (2018) carried out a series of assimilation experiments that run from 10 to 1990 CE, with data from the field models assimilated every 20 years. The goal of these experiments is to determine whether the *CALS3k.4* field model can have a positive impact on the forecasting of the later fields, particularly CM4. About 20 numerical experiments were done, in which the maximum degree (L_{assim}) assimilated and/or the observation error coefficient (α^o) for *CALS3k.4* were varied. In all cases the assimilation is done every 20 years, and geodynamo model parameters used are $R_{th} = 3622$ (or 30 times the critical Rayleigh number for the onset of thermal convection), and an Ekman number $E = 1.25 \times 10^{-6}$.

Here we summarize some of the experimental results from Tangborn and Kuang (2018) in the form of the RMS of the observed minus forecast (O-F) statistics several of the simulations over 2000 years (Figure 19.5), and the RMS O-F at the end of the simulations in 1990 for all of the simulations (Figure 19.6). In all experiments, observations up to degree $L = 8$ are assimilated after 1590 (when *gufm1* begins) with much smaller observation error estimates. Figure 19.5 shows trajectories of the RMS (O-F) over 2000 years, for 3 different maximum degree (L) of Gauss coefficients assimilated ($L = 2, 3, 4$). And it shows that, for the observation model used, the most accurate case is with a maximum of $L = 3$ assimilated. This implies that there is useful information in the *CALS3k.4* field model prior to 1590 that is useful in making geomagnetic forecasts in 1990. The RMS O-F values from 1990 for the complete set of assimilation experiments are shown in Figure 19.6. Here both the maximum

degree assimilated for *CALS3k.4* and the observation error coefficient, α^o, are varied. This indicates that the maximum assimilated degree of $L = 3$ produces the best forecast in 1990, from the experiments carried out, even though the *gufm1* and CM4 observation errors used are the same in all cases.

19.6 Concluding remarks

In this chapter we have reviewed recent research efforts for prediction of geomagnetic variations on different time scales. We used the two very contrasting examples, the weak periodic geomagnetic anomalies from tides and the strong chaotic SV from the outer core, to explain the physics and the mathematics used for the prediction, the progresses made in SV forecasts, and the challenges for future development.

The observables and their error-covariance matrices in (19.6) and (19.7) come from field modeling efforts in which the poloidal core coefficients are separated from other sources. This is key to provide the assimilation algorithm with the proper data and realistic uncertainties. There are several ways in which this field separation can interact with GDAS. One is to parameterize the poloidal core coefficients in terms of empirical temporal basis functions and subsequently provide the assimilation with the resulting coefficient time series and error-covariance. Another approach is to use magnetic measurements as the observables and include non-core sources in the state variables. Either way helps to mitigate bias in the core poloidal field estimates.

While tidal magnetic fluctuations are very weak in amplitude relative to that of SV, they dominate the variability seen in the diurnal to semi-diurnal frequencies. Agreement between theoretical forward models and field models based in observations present at least the primary semi-diurnal lunar tidal fluctuations as highly predictable in at least the coarse features. It is similarly expected that forward modeling of weaker ocean tidal magnetic fields is predictive, though this has yet to be confirmed. The "tidal" magnetic fields associated with solar heating of the upper atmosphere are expected and observed to be less stationary. Despite this, analyses of pre-whitened ground magnetic observatory data show that much if not most of the variance is organized with respect to the solar day and is modulated by the solar cycle. It seems then that much of the geomagnetic variability at quasi-diurnal frequencies and the associated harmonics can be deterministically related to astronomical spin/orbit

parameters and solar variability. Claims in this regard must also consider regional variations as competing unresolved signals may pose limitations at high latitudes and equatorial regions.

As described in Section 19.5, the relative geomagnetic anomalies defined in (19.10) from geodynamo simulation have displayed asymptotically convergence in both the magnitude (see the mean and the standard deviation in Table 19.1) and the time scales (see the power spectra in Figure 19.4). These can be used to define the scaling relations between the non-dimensional magnetic field from geodynamo simulation and the core field derived from geomagnetic measurements. In particular, asymptotic convergence of the spectra of the magnetic anomalies (in Figure 19.4) can be used to estimate the time resolutions of geodynamo models, and thus the limit of forecast shortest geomagnetic variations from the outer core, such as occurrence of geomagnetic jerks (on sub-annual time scales).

Further improvement in SV prediction relies on improving knowledge of error statistics of geomagnetic field models and geodynamo models, in particular the biases than cannot be described by covariance matrices. But the biases in both modeling are affected by the knowledge of the core dynamics, which is that is only partially built into geodynamo modeling, and partially (and empirically) implemented in geomagnetic field modeling. The two fragments may not be consistent. And assimilation of the two models could certainly lead to erroneous estimation of the core state. An attractive approach to reduce such inconsistencies (and therefore biases) is to integrate both modeling effort, such that the field models are used to make initial forecasts; the forecasts are then fed back to improve the field models, which will be used again for improved forecasts. The iterations will continue, until an optimal solution is reached. This approach is conceptually similar to the parameter "co-estimation" used in geomagnetic field modeling (see Section 19.2), but on model "co-development". Therefore we name this approach the "dynamic field modeling". However, a large ensemble of field models and geodynamo models may be needed to make this to work, thus requiring a community effort.

The long term (2000 years) assimilation experiments point to the conclusion that over more than a millennium, observational information from field models is retained in the numerical geodynamo model so as to improve modern day geomagnetic forecasts. And because this information is not lost from the model over these long time periods, there remains some hope that longer term forecasts can also be made. The work of Morzfeld et al (2017) using a simple scalar model adds to the

evidence that this may be possible. However, this may require a numerical model that lies in between these two approaches in complexity and computational cost.

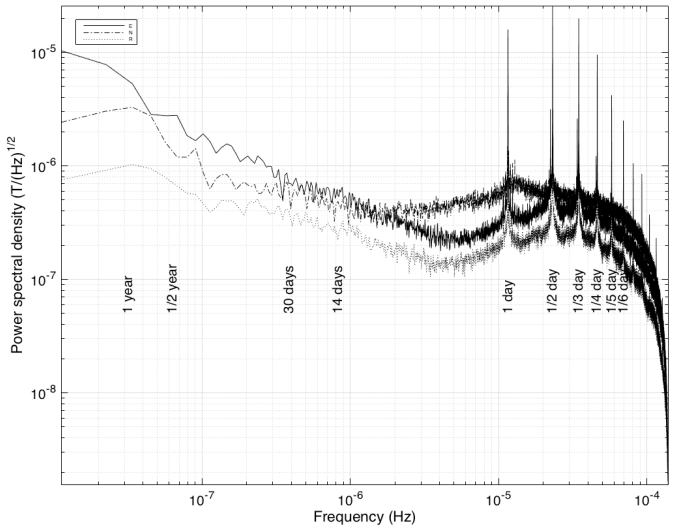

Figure 19.1 Eastward (E), Northward (N), and Radial (R) vector components of the time-rate of change of geomagnetic observations at the Honolulu observatory.

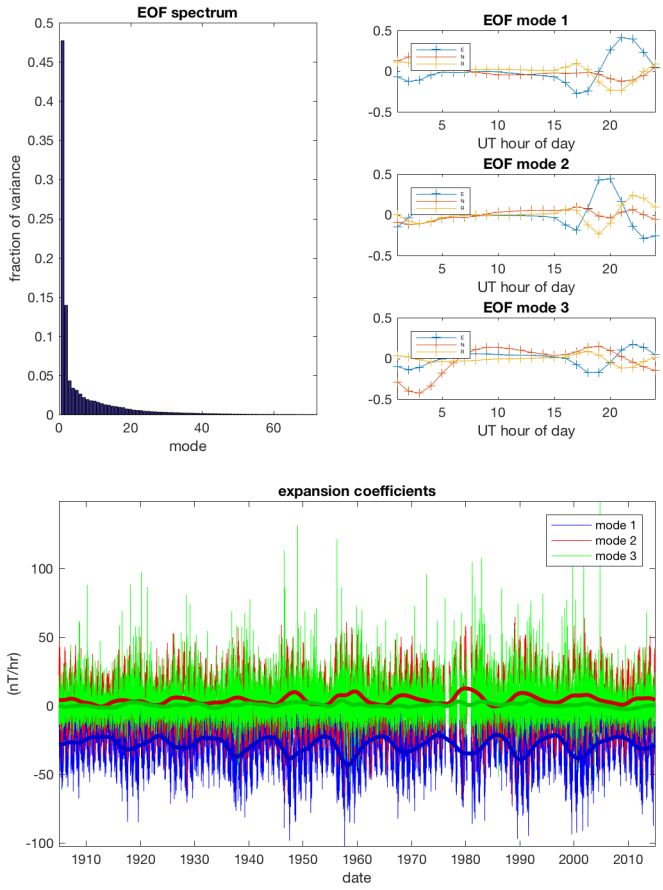

Figure 19.2 EOF analyses of the day vs. hour data matrix of geomagnetic data from Honolulu. The EOF spectrum (upper left panel) shows that more than half of the variance is explained by the first two EOF modes; the EOFs (daily structures of E, N, R) for the first three modes are shown in the upper right panel. The associated expansion coefficients (lower panel) of the first two modes primarily show a seasonal cycle modulated by the solar cycle (as indicated by the thicker curves obtained by low-pass filtering the series with a three-year moving window). Because seasons as well as the solar cycle can be predicted, around half of the variance E, N, R is expected to also be predictable using only the first two EOF modes.

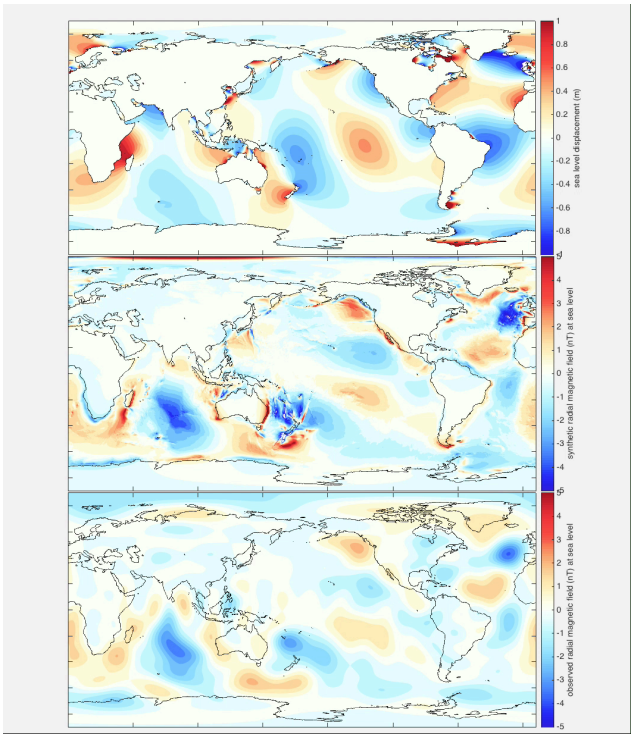

Figure 19.3 Movie frame of M_2 tidal surface displacement (top frame), and the radial component of magnetic field generated by the tidal flow as calculated in a numerical model (middle frame) and as seen in observations (bottom frame). The agreement between the bottom two frames strongly supports the assumption that the observed M_2 magnetic fluctuations are primarily due to ocean tides.

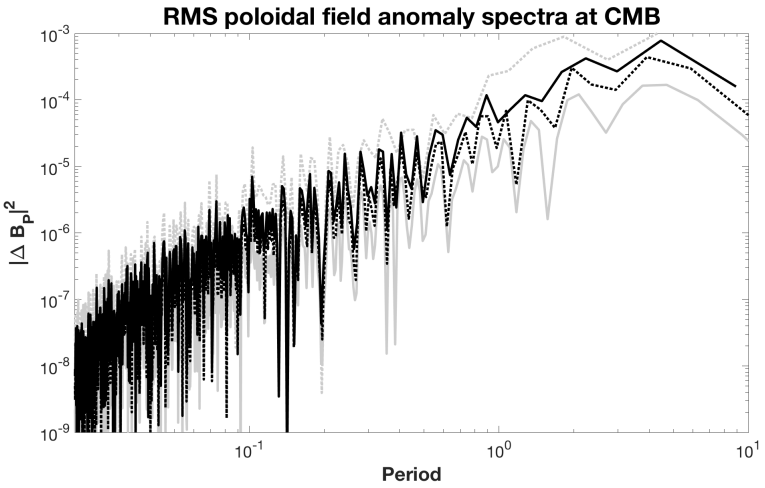

Figure 19.4 The power spectra of the time series δB_P of the poloidal field $\mathbf{B}_P$ at the top of the $D''-$layer defined in (19.10) for $R_o = 2.15\times 10^{-6}$ (dotted gray), 1.25×10^{-6} (solid gray), 6.25×10^{-7} (dotted black) and 3.125×10^{-7} (black). The horizontal axis is the non-dimensional period (the unit period is equivalent to the magnetic free-decay time $\tau_d \approx 20000$ years for the Earth).

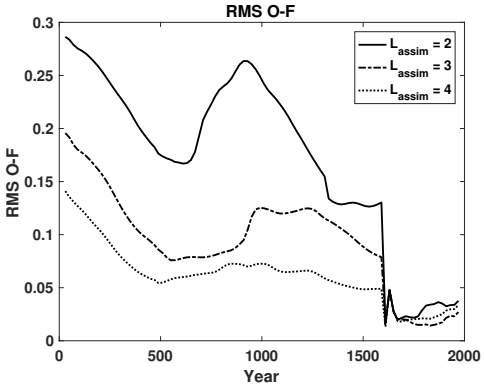

Figure 19.5 $RMS(\mathbf{V}_k)$ of 20 year forecasts for degrees up to $L = 3$, for assimilation runs starting in 10 CE and finishing in 1990 CE. In all cases the observation error is set to $\sigma^o = 1.0|b_L^m|$ (so $\alpha^o = 1.0$), and coefficients are assimilated up to degree $L_{assim} = 2$ (black), $L = 3$ (dashed) and $L = 4$ (dotted).

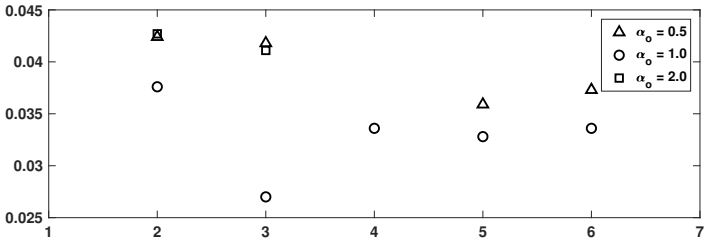

Figure 19.6 $RMS(\mathbf{V}_k)$ of 20 year forecasts in 1990, for all of the assimilation experiments starting in 10 CE and finishing in 1990 CE. The x-axis shows the maximum degree L assimilated, and the observation error coefficient used up to 1590, σ^o, is indicated by the symbols in the legend (from 0.5 to 2).

References for Chapter 19

Aubert, J. 2014. Earth's core internal dynamics 1840−2010 imaged by inverse geodynamo modelling. *Geophys. J. Int.*, **197**, 1321–1334.

Aubert, J. and Fournier, A. 2011. Inferring internal properties of Earth's core dynamics and their evolution from surface observations and a numerical geodynamo model. *Nonlinear Process. Geophys.*, **18**, 657–674.

Aubert, J., Gastine, T. and Fournier, A. 2017. Spherical convective dynamos in the rapidly rotating asymptotic regime. *J. Fluid. Mech.*, **813**, 558-593.

Barrois, O., Gillet, N. and Aubert, J. 2017. Contributions to the geomagnetic secular variation from a reanalysis of core surface dynamics. *Geophys. J. Int.*, **211** 50–68.

Beggan, C. D. and Whaler, K. A. 2009. Forecasting change of the magnetic field using core surface flows and ensemble Kalman filtering. *Geophys. Res. Lett.*, doi:10.1029/2009GL039927.

Bouligand,C., Gillet, N., Jault, D., Schaeffer, N. Fournier, A. and Aubert, J. 2016. Frequency spectrum of the geomagnetic field harmonic coefficients from dynamo simulations. *Geophys. J. Int.*, **207**, 1142–1157.

Canet, E., Fournier, A. and Jault, D. 2009. Forward and adjoint quasi-geostrophic models of the geomagnetic secular variation. *J. Geophys. Res.*, doi:10.1029/2008JB006189.

Christensen, U. R., Aubert, J., Cardin, P., Dormy, E., Gibbons, S., Glatzmaier, G. A., Grote, E., Honkura, Y, Jones, C., Kono, M., Matsushima, M., Sakuraba, A., Takahashi, F., Tilgner, A., Wicht, J., Zhang, K. 2001. A numerical dynamo benchmark *Phys. Earth Planet. Inter.*, **128**, 25–34.

Christensen, U. R., Aubert, J. and Hulot, G. 2010. Conditions for Earth-like geodynamo models. *Earth Planet. Sci. Lett.*, **296**, 487–496.

Colosi, J. A. and Munk, W. 2006. Tales of the Venerable Honolulu Tide Gauge. *J. Phy. Oceano.*, **36**, 967–996.

Donadini, F., Korte, M. and Constable, C. G. 2009. Geomagnetic field for 0-3 ka: 1. New data sets for global modeling. *Geochem. Geophys. Geosys.*, **10**, Q06007, doi:10.1029/2008GC002295.

Egbert, G. P. and Ray, R. D. 2017. Tidal Prediction. *Journal of Marine Research*, **189-237**, 1–49.

Finlay, C.C., Lesur, V., TThébault, E., Vervelidou, F., Morschhauser, A. and Shore, R. 2017. Challenges handling magnetospheric and ionospheric signals in internal geomagnetic field modeling, *Space Sci. Rev.* , **206**, 157-189. doi:10.10007/s11214-016-0285-9.

Finlay, C.C., Olsen, N., Kotsiaros, S., Gillet, N. and Toffner-Clausen, L. 2016. Recent geomagnetic secular variation from Swarm and ground observatories as estimated in the CHAOS-6 geomagnetic field model. *Earth, Planets and Space*, **68**. doi:10.1186/s40623-016-0486-1.

Fournier, A., Eymin, C. and Alboussiere, T. 2007. A case for variational geomagnetic data assimilation: insights from a one-dimensional, nonlinear, and sparsely observed MHD system. *Nonlin. Processes Geophys.*, **14**, 163–180.

Fournier, A., Hulot, G., Jault, D., Kuang, W., Tangborn, A., Gillet, N., Canet, E., Aubert, J. and Lhuillier, F. 2010. An introduction to data assimilation and predictability in geomagnetism. *Space Sci. Rev.*, **155**, 247–291.

Fournier, A., Aubert, J. and Thébault, E. 2011. Inference on core surface flow from observations and 3-D dynamo modelling. *Geophys. J. Int.*, **186**, 118–136.

Fournier, A., Nerger, L. and Aubert, J. 2013. An ensemble Kalman filter for the time-dependent analysis of the geomagnetic field. *Geochem. Geophys. Geosys.*, doi:10.1002/ggge.20252.

Fournier, A., Aubert, J. and Thébaut, E. 2015. A candidate secular variation model for IGRF-12 based on Swarm data and inverse geodynamo modeling. *Earth, Planets and Space*, **67**, doi 10.1186/s40623-015-0245-8.

Gillet, N., Jault, D., Canet, E. and Fournier, A. 2010. Fast torsional waves and strong magnetic field within the Earth's core. *Nature*, doi:10.1038/nature09010.

Gillet, N., Jault, D., Finlay, C. C. and Olsen, N. 2013. Stochastic modeling of the Earth's magnetic field: Inversion for covariances over the observatory era. *Geochem. Geophys. Geosys.*, doi:10.1002/ggge.20041.

Gillet, N., Barrois, O., and Finlay, C. C. 2015. Stochastic forecasting of the geomagnetic field from the COV-Obs.x1 geomagnetic field model, and candidate models for IGRF-12. *Earth, Planets and Space*. doi:10.1186/s40623-015-0225-z.

Grayver, A. V., Schnepf, N. R., Kuvshinov, A. V., Sabaka, T. J., Manoj, C. and Olsen, N. 2016 Satellite tidal magnetic signals constrain oceanic lithosphere-asthenosphere boundary. *Sci. Adv.*, doi:10.1126/sciadv.1600798.

Grayver, A. V., Munch, F. D., Kuvshinov, A. V., Khan, A., Sabaka, T. J. and Tøffner-Clausen, L. 2017. Joint inversion of satellite-detected tidal and magnetospheric signals constrains electrical conductivity and water content of the upper mantle and transition zone. *Geophys. Res. Lett.*, doi:10.1002/2017GL073446.

Hammill, T. M., Snyder, C., A Hybrid Ensemble Kalman Filter3D Variational Analysis Scheme. *Mon. Wea. Rev.*, **128**, 2905-2915.

Holme, R. and Whaler, K. A. 2001. Steady core flow in an azimuthally drifting reference frame. *Geophys. J. Int.*, **145**, 560–569.

Hulot, G., Lhuillier, F. and Aubert, J. 2010. Earth's dynamo limit of predictability. *Geophys. Res. Lett.*, **37**, doi:10.1029/2009GL041869.

Jackson, A., Jonkers, A. R. T. and Walker, M. R. 2000. Four centuries of geomagnetic secular variation from historical records. *Phil. Trans. R. Soc. Lond.*, **A358**, 957–990.

Jault, D., Gire, C. and LeMouël, J.-L. 1988. Westward drift, core motions and exchanges of angular momentum between core and mantle. *Nature*, **333**, 353–356.

Jault, D. 2013. Axial invariance of rapidly varying diffusionless motions in the Earth?s core interior. *Phys. Earth Planet. Inter.*, **166**, 67–76.

Jiang, W. and Kuang, W. 2008. An MPI-based MoSST core dynamics model. *Phy. Earth Planet. Inter.*, **170**, 46–51.

Jones, C. A., Boronski, P., Brun, A. S. Glatzmaier, G. A., Gastine, T., Miesch, M. S. and Wicht, J. 2011. Anelastic convection-driven dynamo benchmarks. *Icarus*, **216**, 120–135.

Kalnay, E. 2011. *Atmospheric Modeling, Data Assimilation and Predictability*, 7th edition. Cambridge University Press.

Korte, M. and Constable, C. G. 2005. The geomagnetic dipole moment over the last 7000 years – new results from a global model. *Earth Planet. Sci. Lett.*, **236**, 348–358.

Korte, M. and Constable, C. G. 2011. Improving geomagnetic field reconstructions for 0–3 ka. *Phys. Earth Planet. Inter.*, **188**, 247–259.

Kuang, W. and Bloxham, J. 1997. An Earth like numerical dynamo model. *Nature*, **389**, 371–374.

Kuang, W. and Bloxham, J. 1999. Numerical modeling of magnetohydrodynamic convection in a rapidly rotating spherical shell: weak and strong dynamo action. *J. Comp. Phys.*, **153**, 51–81.

Kuang, W., and Chao, B. F. 2003. Geodynamo modeling and core-mantle interactions. In: Dehant, V., Kreager, K. C., Karato, S., and Zatman, S. (eds), *Earth's Core: Dynamics, Structure, Rotation*, Geodynamics Series **31**. American Geophysics Union, Washington, D.C.

Kuang, W., and Tangborn, A. 2015. Dynamic responses of the Earth's outer core to assimilation of observed geomagnetic secular variation. *Prog. Earth Planet. Sci.*, doi: 10.1186/s40645-015-0071-4.

Kuang, W., Tangborn, A., Jiang, W., Liu, D., Sun, Z., Bloxham, J. and Wei, Z. 2008. MoSST_DAS: the first generation geomagnetic data assimilation framework. *Commu. Comp. Phys.*, **3**, 85–108.

Kuang, W., Wei, Z., Holme, R. and Tangborn, A. 2010. Constraining a numerical geodynamo model with 100 years of surface observations. *Geophys. J. Int.*, doi:10.1111/j.1365-246X.2009.04376.x.

Kuang, W., Tangborn, A., Wei, Z. and Sabaka, T. 2009. Prediction of geomagnetic field with data assimilation: a candidate secular variation model for IGRF-11. *Earth Planets Space*, **62**, 775–785.

Kuang, W., Chao, B. F. and Chen, J. 2017. Decadal polar motion of the Earth excited by the convective outer core from geodynamo simulations. *J. Geophys. Res.*, (accepted).

Langel, R. A. 1987. The main geomagnetic field. In: Jacobs, J. A. (eds), *Geomagnetism*, Vol. 1. Academic Press, London.

Lesur, V., Wardinski, I., Rother, M. and Mandea, M. 2008. GRIMM: the GFZ Reference Internal Magnetic Model based on vector satellite and observatory data. *Geophys J Int.*, **173**, 382–394.

Lesur, V., Rother, M. Wardinski, I., Schachtschneider, R., Hamoudi, M. and Chambodut, A. 2015a. Parent magnetic field models for the IGRF-12: GFZ-candidates. *Earth Planets Space*, doi:10.1186/s40623-015-0239-6.

Lesur, V., Whaler, K. and Wardinski, I. 2015b. Are geomagnetic data consistent with stably stratified flow at the core-mantle boundary? *Geophys. J. Int.*, doi:10.1093/gji/ggv031.

Li, K., Jackson A. and Livermore, P. W. 2011. Variational data assimilation for the initial-value dynamo problem. *Phys. Rev. E*, **84**, doi: 10.1103/PhysRevE.84.056321.

Li, K., Jackson A. and Livermore, P. W. 2014. Variational data assimilation for a forced, inertia-free magnetohydrodynamic dynamo model. *Geophys. J. Int.*, **199**, 1662-1676.

Licht, A., Hulot, G., Gallet, Y. and Thébault, E. 2013. Ensembles of low degree archeomagnetic field models for the past three millennia *Phys. Earth Planet. Inter.*, **224**, 38–67.

Liu, D., Tangborn, A. and Kuang, W. 2007. Observing system simulation experiments in geomagnetic data assimilation. *J. Geophys. Res.*, **112**, doi:10.1029/2006JB004691.

Love, J. J. and Rigler, E. J. 2014. The magnetic tides of Honolulu. *Geophys. J. Int.*, **197**, 1335–1353.

Matsui, H. Heien, E., Aubert, J., Aurnou, J. M., Avery, M., Brown, B., Buffett, B. A., Busse, F., Christensen, U. R., Davies, C. J., Featherstone, N., Gastine, T., Glatzmaier, G. A., Gubbins, D., Guermond, J.-L., Hayashi, Y., Hollerbach, R., Hwang, L. J., Jackson, A., Jones, C. A., Jiang, W., Kellogg, L. H., Kuang, W., Landeau, M., Marti, P., Olson, P., Ribeiro, A., Sasaki, Y., Schaeffer, N., Simitev, R. D., Sheyko, A., Silva, L., Stanley, S., Takahashi, F., Takehiro, S., JWicht, J., and Willis, A. P. 2016. Performance benchmarks for a next generation numerical dynamo model. *Geochem. Geophys. Geosys.*, doi: 10.1002/2015GC006159

Maus, S. 2017. POMME-9 magnetic model of the Earth. *http://geomag.colorado.edu/pomme-9-magnetic-model-of-the-earth.html.*

Maus, S., Macmillan, S., Lowes, F. and Bondar, T. 2005. Evaluation of candidate geomagnetic field models for the 10th generation of IGRF. *Earth Planets Space*, **57**, 1173–1181.

Maus, S., Rother, M., Stolle, C., Mai, W., Choi, S., Lühr, H., Cooke, D. and Roth, C. 2006. Third generation of the Potsdam Magnetic Model of the Earth (POMME). *Geochem. Geophy. Geosys.*, doi:10.1029/2006GC001269.

Maus, S., Silva, L. and Hulot, G. 2008. Can core-surface flow models be used to improve the forecast of the Earth's main magnetic field? *J. Geophys. Res.*, doi:10.1029/2007JB005199.

Morzfeld, M., Fournier, A. and Hulot, G. 2017. Coarse predictions of dipole reversals by low-dimensional modeling and data assimilation. *Phys. Earth Planet. Inter.*, **262**, 8–27.

Nilsson, A., Holme, R., Korte, M., Suttie, N. and Hill, M. 2014. Reconstructing Holocene geomagnetic field variation: new methods, models and implications. *Geophys. J. Int.*, doi: 10.1093/gji/ggu120.

Olsen, N. and Stolle, C. 2017. TMagnetic signatures of ionospheric and magnetospheric current systems during geomagnetic quiet conditions – an overview. *Space Sci. Rev.*, **206**, 5–25. doi: 10.1007/s11214-016-0279-7.

Olsen, N., Lühr, H., Finlay, C. C., Sabaka, T. J., Michaelis, I., Rauberg, J. and Tøffner-Clausen, L. 2014. The CHAOS-4 geomagnetic field model. *Geophys. J. Int.*, **197**, 815–827.

Sabaka, T. J. and Olsen, N. 2006. Enhancing comprehensive inversions using the *Swarm* constellation. *Earth Planets Space*, **58**, 371–395.

Sabaka, T. J., Olsen, N. and Langel, R. A. 2002. A comprehensive model of the quiet-time, near-Earth magnetic field: phase 3. *Geophys. J. Int.*, **151**, 32–68.

Sabaka, T. J., Olsen, N. and Purucker, M. E. 2004. Extending comprehensive models of the Earth's magnetic field with Ørsted and CHAMP data. *Geophys. J. Int.*, **159**, 521–547.

Sabaka, T. J., Tøffner-Clausen, L. and Olsen, N. 2013. Use of the Comprehensive Inversion method for *Swarm* satellite data analysis. *Earth Planets Space*, **65**, 1201–1222.

Sabaka, T. J., Olsen, N., Tyler, R. H. and Kushinov, A. 2015. CM5, a pre-*Swarm* comprehensive geomagnetic field model derived from over 12 yr of CHAMP, Ørsted, SAC-C and observatory data. *Geophys. J. Int.*, **200**, 1596–1626.

Sabaka, T. J., Tyler, R. H. and Olsen, N. 2016. Extracting ocean-generated tidal magnetic signals from *Swarm* data through satellite gradiometry. *Geophys. Res. Lett.*, doi:10.1002/2016GL068180.

Sakuraba, A. and Roberts, P. H. 2009. Generation of a strong magnetic field using uniform heat flux at the surface of the core. *Nature Geosci.*, doi: 10.1038/NGEO643.

Sanchez,S., Fournier, A., Aubert, J. and Gallrt, Y. 2016. Modelling the archaeomagnetic field under spatial constraints from dynamo simulations: a resolution analysis. *Geophy. J. Int.*, **207** 983–1002.

Schnepf, N. R., Kuvshinov, A. and Sabaka, T. J. 2015. Can we probe the conductivity of the lithosphere and upper mantle using satellite tidal magnetic signals? *Geophys. Res. Lett.*, doi:10.1002/2015GL063540.

Sun, Z., Tangborn, A. and Kuang, W. 2007. Data assimilation in a sparsely observed one-dimensional modeled MHD system. *Nonlin. Processes Geophys.*, **14**, 181–192.

Sun, Z. and Kuang, W. 2015. An ensemble algorithm based component for geomagnetic data assimilation. *Terr. Atmos. Ocean. Sci.*, **26**, 53–61.

Tangborn, A. and Kuang, W. 2015. Geodynamo model and error parameter estimation using geomagnetic data assimilation *Geophys. J. Int.*, **200**, 664–675.

Tangborn, A. and Kuang, W. 2018. Impact of archeomagnetic field model data on modern era geomagnetic forecasts. *Phys. Earth and Planet. Inter.*, **276**, 2-9.

Tyler, R. H. 2013. Magnetic Remote Sensing of Ocean Flow Variability. In: *IAGA 12th Scientific Assembly, Living on a Magnetic Planet. Merida, 26-31 August, 2013.*

Tyler, R. H., Maus, S. and Lühr, H. 2003. Satellite observations of magnetic fields due to ocean tidal flow *Science*, **299**, 239–241.

Tyler, R. H., Boyer, T. P., Minami, T., Zweng, M. M. and Reagan, J. R. 2017. Electrical conductivity of the global ocean. *Earth Planets Space* (submitted).

Whaler, K. A. and Beggan, C. D. 2015. Derivation and use of core surface flows for forecasting secular variation. *J. Geophys. Res.: Solid Earth*, doi:10.1002/2014JB011697.

Author index

Subject index